Prediction of Grain Size, Precipitation and Crack Susceptibility in Continuous Casting

Kun Xu, Brian G. Thomas
Mechanical Science and Engineering Department
University of Illinois at Urbana-Champaign
1206 West Green St., Urbana, IL 61801, USA
Phone – (217) 333-6919
Fax – (217) 244-6534
E-mail: kunxu2@illinois.edu, bgthomas@illinois.edu

Key Words: Precipitate formation, continuous casting, oscillation marks, equilibrium precipitation, particle-size-grouping method, grain growth, boundary pinning force

ABSTRACT

The formation of precipitates, especially along austenite grain boundaries, greatly affects the formation of transverse cracks on the surface of continuous-cast steel. The steel composition and cooling history influences the formation of precipitates, and the higher temperature and corresponding larger grain growth rate under oscillation marks or surface depressions also have an important effect on crack problems. This paper develops a model to predict and track the amount, composition and size distribution of precipitates and the grain size in order to predict the susceptibility of different steel grades to ductility problems during continuous casting processes. The results are important for controlled cooling of microalloyed steels to prevent cracks and assure product quality.

INTRODUCTION

The demand for steels with higher strength, ductility and toughness is always increasing. Many alloy additions aim to improve these final product properties by controlling grain size and precipitate formation during rolling operations. Large grain size decreases ductility and toughness, by allowing strain to concentrate at the grain boundaries to form cracks. Alloys often act by promoting a dispersion of very fine precipitate particles, and/or by inhibiting grain growth through these second-phase particles. An unfortunate side effect is a decrease in high temperature ductility and crack formation during the casting process, which is governed by similar mechanisms. The amount, composition, morphology and size distribution of precipitates evolving from the molten steels to the final products are important for determining the mechanical properties of modern commercial steels throughout processing. Precipitation and grain size are both influenced greatly by the steel composition and cooling history. There is a critical balance for precipitates to form and function. If dissolved or too fine, they will have no effect. If they grow too large, they will not restrict grain boundary movement and corresponding growth, and will themselves cause quality problems. It is important to control primary and secondary cooling during the casting process to produce optimal temperature and stress histories that avoid subjecting the steel strand to high strains during those critical time periods when the grain size is large, embrittling precipitates are present and the steel is susceptible to crack formation.

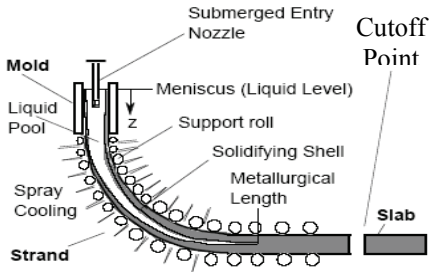

Figure 1. Schematic of continuous casting process

Figure 1 shows a typical continuous casting process in the steel industry. After cooling in the mold, the strand moves through spray zones, where the water flow rates are controlled to achieve a desired temperature history in the solidifying shell. High-speed thin-slab

casters save energy relative to conventional low-speed ones. However, the shorter times and generally higher temperatures change the metallurgical behavior, including grain size, precipitate formation, high-temperature ductility, and susceptibility to surface cracks. Thus, there is a strong need for accurate predictive tools to help design cooling practices to avoid cracks and to maximize surface quality.

Objectives

This paper introduces a comprehensive project to develop a fundamentally-based model of the continuous casting process to predict embrittlement and crack susceptibility for different steel grades and cooling practices, based on a quantitative prediction of the steel microstructure. The first step is to predict temperature and phase fraction history throughout the strand during the process using an existing model, CON1D. Then an equilibrium precipitation model and kinetic model are developed to predict the composition, volume fraction and size distribution of precipitates. In addition, a grain growth model is being developed to simulate the austenite grain size, including the pinning effect of precipitates, temperature and time space.

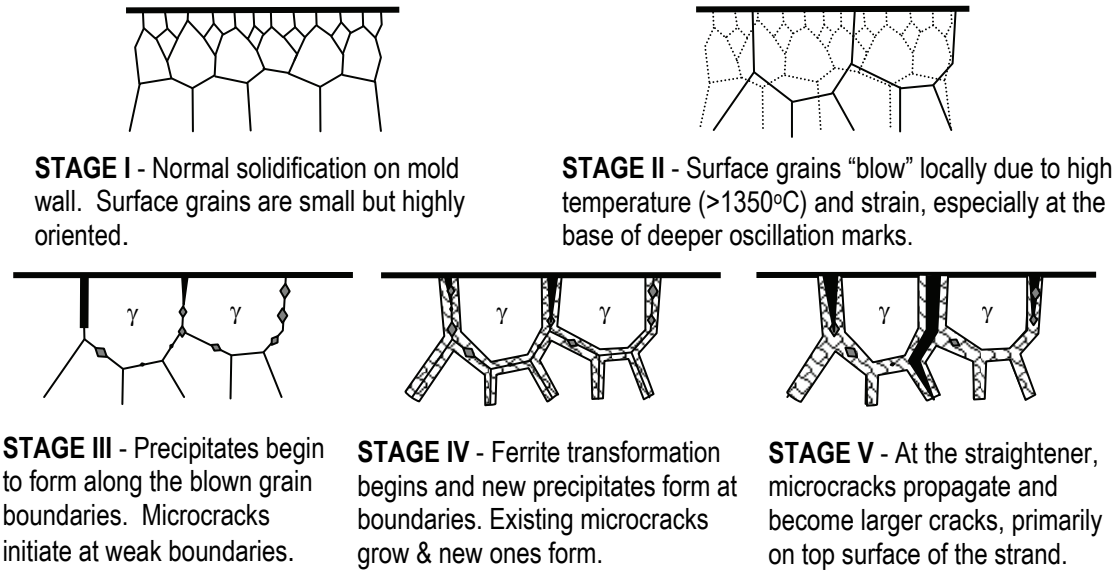

STAGE I - Normal solidification on mold wall. Surface grains are small but highly oriented.

STAGE II - Surface grains "blow" locally due to high temperature (>1350°C) and strain, especially at the base of deeper oscillation marks.

STAGE III - Precipitates begin to form along the blown grain boundaries. Microcracks initiate at weak boundaries.

STAGE IV - Ferrite transformation begins and new precipitates form at boundaries. Existing microcracks grow & new ones form.

STAGE V - At the straightener, microcracks propagate and become larger cracks, primarily on top surface of the strand.

Figure 2. The formation of surface cracks and precipitate embrittlement [1]

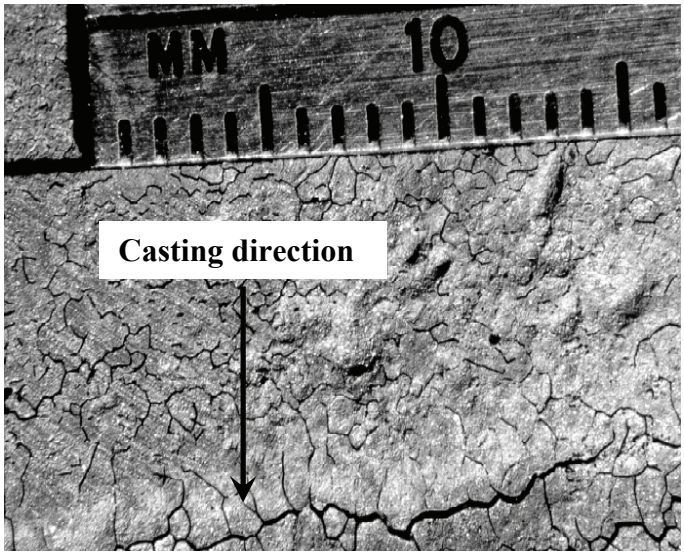

Figure 3. Transverse crack at the base of an oscillation mark of a 0.2% carbon steel slab [1]

Surface Crack Formation Mechanisms

A typical mechanism for transverse surface crack formation is shown in **Figure 2** [1]. Surface grains can grow extremely large due to locally high temperature and strain, especially beneath deep oscillation marks. During casting, precipitates first begin to form along these "blown" grain boundaries and microcracks initiate at the weakened boundaries. With more precipitation, existing microcracks grow and new ones form, and finally propagate into visible cracks on the top surface of the strand. **Figure 3** displays the obviously larger grains and a corresponding transverse crack at the base of an oscillation mark of a 0.2% carbon steel slab, which prove this mechanism of crack formation during continuous casting.

Thermodynamic Models of Equilibrium Precipitation

The first crucial step to predict precipitate formation, composition and growth is a thermodynamic analysis to predict the equilibrium precipitate phases and their compositions present for any steel grade and temperature. This is critical for calculating supersaturation. Many researchers have tried to solve this problem by establishing equations based on experimentally measured solubility products of precipitates of interest. Liu [2] developed a method to compute the equilibrium precipitation state in microalloyed steel, which solved mass balances together with solubility products, but without consideration of mutual solubility. Park [3] calculated the equilibria between austenite and MnS sulfides in the presence of sulfides as $Ti_4C_2S_2$, TiS and carbonitrides as $Ti_xV_{1-x}C_yN_{1-y}$. The sulfides and carbonitrides are assumed mutually insoluble, and stoichiometry is assumed to hold for all sulfides and carbonitrides for simplicity. The Wagner effects for activities are also neglected since the austenite is assumed to be very dilute.

Previous models often make simplifying assumptions, such as equivalent molar fraction for the alloying and interstitial elements for precipitation, and neglect of mutually soluble properties or influence of activities. Thus, they are only suitable for specific steel grades and precipitates. Several Gibbs Energy minimization software packages, such as ThermoCalc [4,5], CALPHAD [6,7], FactSage [8], and ChemSage [9] have been used to analyze precipitation behaviors. These packages can perform thermodynamic calculations for precipitation in multi-component steels. Although these packages can predict the occurrence, sequence and equilibrium composition of some precipitates, and have been validated with some experimental results, the accuracy of the solubility databases and general applicability for other precipitate types, especially those which are mutually-soluble, is still in question. Furthermore, they cannot be used to predict precipitate formation and their size distributions, in real castings, where nonequilibrium effects, such as delays due to diffusion kinetics, are very important.

Kinetic Models of Precipitate Growth

Precipitates can form in different stages and locations, including in the liquid steel due to collision, the mushy-zone between dendrites due to rapid diffusion during solidification, and on the grain boundaries or inside the grains due to slow solid-state diffusion. The particles can have different composition, morphology and size distribution, which greatly affects their influence on properties. The formation of precipitates may be sluggish even if they are thermodynamically favored, so a kinetic model is essential.

Precipitate particles grow via two major mechanisms: collision in liquid [10,11,12] and diffusion (Ostwald Ripening) in both liquid and solid [13,14,15]. Both mechanisms have been studied extensively, and better computational models are now available.

However, practical models of particle growth must simulate from nuclei (~0.1nm) to large coarsened particles (~100μm). This particle size ranges from ~1 to ~10^{18} elementary molecules, which presents a prohibitive computational cost for any method based on a linear size scale.

In order to overcome this problem, the particle-size-group (PSG) method has been developed. Nakaoka *et al.* [16] modeled agglomeration behavior theoretically to validate the PSG method for different volume ratios between neighboring size groups. The numerical results agreed well with experimental agglomeration curves of PVTL for various particle concentration and agitation speeds. Zhang [17] applied a PSG collision model with intra-group interactions coefficients very recently. However, problems remain involving conservation of total mass and interactions within size groups. Furthermore, the PSG method has only been applied to collisions, and not to diffusion, which is the dominant mechanism for particle growth in the solid sate of steels.

Grain Size Prediction

The microstructure strongly affects steel mechanical properties, so predicting grain size is an essential component of an accurate model. In addition to thermally-activated mechanisms, grain growth depends strongly on the presence of growing and dissolving precipitates. Grain size control through the pinning of grain boundaries with microalloyed precipitates is widely applied to improve steel properties in commercial practice. Andersen and Grong[18,19] established differential equations for grain growth in metal alloys which can be integrated in temperature and time space to give the matrix grain size, accounting for the pinning force of precipitates . Reiter and Bernhard [21] applied this model to predict austenite grain size in laboratory experiments, while neglecting precipitate effects because of high cooling rate. By carefully choosing physical parameters, a good match was achieved between calculated and measured grain size in exposed austenite grains using several etching methods [20]. However, most calculations start from austenite with an assumed initial grain size.

Thermodynamic models for predicting the precipitate stability and supersaturation should be linked with kinetic models to describe both the particle size distribution and volume fraction and coupled as the pinning force into the grain growth equation. Furthermore, the analysis should start in the liquid phase, and consider the evolution of the size distributions during solidification between the dendrite arms, in addition to behavior in the solid state.

HEAT TRANSFER MODEL

Temperature and phase fraction development during the solidification and cooling process is the first crucial part of a model system to predict microstructure and ductility. In this work, the transient heat conduction equation is solved in the mold and spray regions of a continuous steel slab caster using the CON1D program [22]. This finite-difference model calculates one-dimensional heat transfer within the solidifying steel shell coupled with two-dimensional steady-state heat transfer in the mold and a careful treatment of the interfacial gap between the shell and mold. Below the mold, the model includes the temperature and spatially-dependent heat transfer coefficients of each spray nozzle, according to the local water flow rates, and the heat extraction into each support roll. A nonequilibrium microsegregation model, based on an analytical Clyne-Kurz equation developed by Won and Thomas [23], was applied to compute the liquidus, solidus temperature and phase fractions. Complete details of CON1D are provided elsewhere [22].
In this work, the casting conditions are chosen to model a typical microalloyed low-carbon 1006 steel in a typical thin slab casting machine, with a 90-mm thick and 950-mm long parallel mold. Details of the spray zone cooling conditions are given elsewhere [24]. Simulations are run for a 1396mm slab width, with 1553°C pour temperature at 3.7 and 5.7 m/min. The calculated temperature and phase fraction histories at the slab surface, at 0.5mm deep, (representing the oscillation mark roots), and at 10mm deep beneath the surface are input to the other models.

EQUILIBRIUM PRECIPITAION MODEL

An equilibrium precipitation model has been developed to predict the onset of precipitation in common steel alloys of oxides, nitrides, sulfides and carbides. It is used to define supersaturation for the precipitate growth model. A fully-coupled system of nonlinear solubility-limit equations is solved for the amounts of each precipitate or mutually-soluble precipitate group, including the influence on activities from the interaction between elements, and complete mass conservation of all elements before and after precipitation.
The solubility product for alloying metal element M and interstitial element X to form compound M_xX_y, is defined as

$$K_{M_xX_y} = a_{[M]}^{x} \cdot a_{[X]}^{y} / a_{(M_xX_y)} \tag{1}$$

Where $a_{[M]}, a_{[X]}, a_{[M_xX_y]}$: Activities of alloying element M, interstitial element X and precipitate M_xX_y

For low solute concentrations, the activity of each element, a_i, is defined by linear Henry's law as

$$a_i = f_i[\%i] \text{ where } \log f_i = e_i^i[\%i] + \sum e_i^j[\%j] \tag{2}$$

Where $[\%i]$, $[\%j]$: Weight percent of dissolved element i and j

e_i^j: Interaction coefficient of element i as affected by the alloying element j

In classic theory, each solid precipitate forms separately with a unique composition, and has an activity of unity in the solid steel. Such precipitates are "mutually exclusive". According to the criterion given in [25], however, a group of precipitates with the same crystal structures and similar lattice parameters (within 10%), will be mutually soluble. Their individual solid activities sum to unity as they always appear and act together.
The commonly observed precipitates considered in this work are divided into groups as *TiNbV(CN)*, *AlTi(O)*, *MnMg(O)*, *MnMg(S)*, *SiO_2*, *TiS*, *$Ti_4C_2S_2$*, *AlN*, *BN*, *Cr_2N*. Currently, there are 18 equations for the solubility limits of 18 precipitates, 13 equations for mass balance of 13 solute elements, and a constraint equation for the coefficients of each of the 4 groups of mutual soluble precipitates. For these 35 equations, there are 35 unknown parameters, including the dissolved concentrations / activities of 13 elements, molar fraction of the 10 groups of precipitates (6 single precipitates and 4 mutually-soluble) and 12 (18-6) mutually soluble coefficients. The complete system of nonlinear equations is solved with a robust Newton method, and is easily modified to include new precipitates or modifications to the thermodynamic data from future research.
The model is first validated with an analytical solution of a simple system of mutually exclusive precipitates in iron: NbN with AlN or BN, as shown in **Figure 4**. The analytical solution of the final second order equations applies with 1:1 ratio of metal element to interstitial element [25]. Precipitates which form first delay the formation of other precipitates if they are mutually exclusive and share the same alloying element. In this case, the stable AlN or BN precipitation postpones NbN to form at lower temperature.
Figure 5 shows simulations of mutually soluble precipitates (NbN with TiN or VN) in three different hypothetical steels. The final equations are at least fourth order so no analytical solution exists. In these steels, the precipitates form as a single group TiNbV(CN), with composition that evolves during cooling, For example, the precipitate group of 69%Ti, 10%Nb and 21%Ti calculated at 1400°C in the Ti-steel, corresponds to the precipitate $Ti_{0.47}Nb_{0.03}N_{0.50}$ by transforming weight percent to molar fractions. As cooling proceeds, the solubility limits decrease and more precipitates form. When Ti is present, TiN precipitates form first, and their fraction decreases with time as NbN forms. This is because TiN is the most stable precipitate (lowest solubility limit), and there is sufficient N in these hypothetical steels to allow the other precipitates to form at lower temperature. With Ti or V additions, another consequence of the mutual solubility is to decrease the equilibrium dissolved concentration of Nb, which allows more NbN precipitate to form. Without consideration of mutual solubility, NbN precipitates would decrease with Ti or V additions.

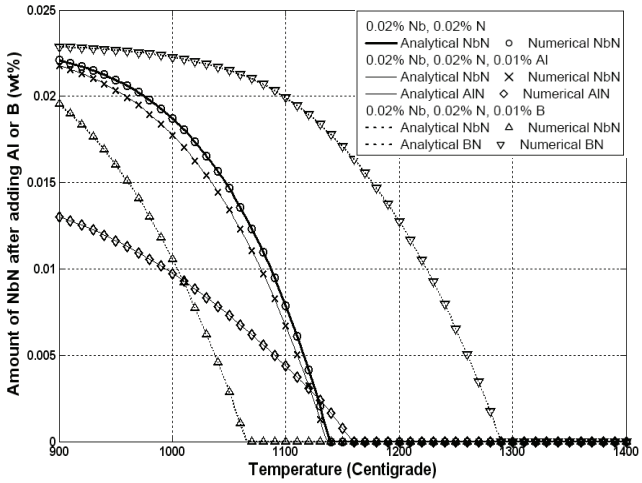

Figure 4. Comparison of equilibrium precipitation with analytical solution in austenite for 3 Fe alloys containing only 0.02%N and 0.02%Nb, and either 0.01% Al or 0.01%B (assuming all precipitates are mutually exclusive)

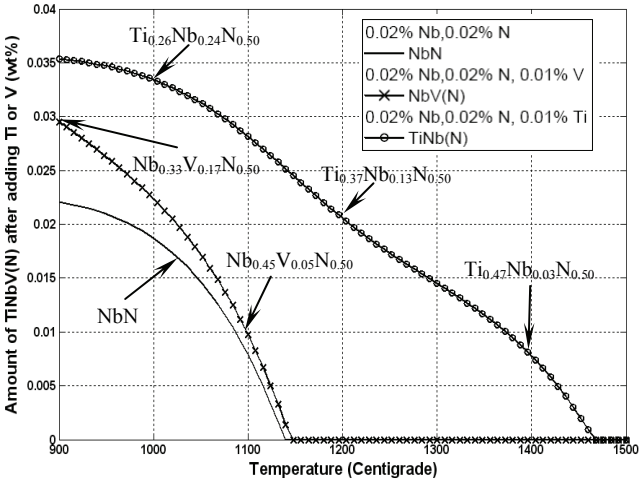

Figure 5. Equilibrium precipitation in austenite for 3 Fe alloys containing only 0.02%N and 0.02%Nb, and either 0.01% Ti or 0.01%V (all mutually soluble precipitates)

Commercial Steel Results

The model is used to analyze the precipitation behavior of continuous casting of a commercial 1006 steel (0.06%C, 1%Mn, 0.2%Si, 0.015%Ti, 0.015% Nb, 0.004%V, 0.006%B, 0.01%N). The temperature history from CON1D with both casting speeds 3.7m/min and 5.7m/min are compared in **Figure 6**. These figures also contain the precipitation amounts predicted by this equilibrium model. TiN is the most stable precipitate, especially at high temperature because of its lowest solubility limit. After most of the N is combined to form the stable nitrides TiN and BN, the Nb has little remaining nitrogen to react with. Consequently, NbC becomes important, because plenty of carbon is available and NbC is mutual solubility with stable TiN. Moreover, the equilibrium concentration of these precipitates varies greatly during secondary cooling, due to the surface temperature fluctuations between rolls.

With higher casting speed, the temperature in the secondary spray zones increases. This has little effect on the TiN content, but greatly lessens the amount of the other precipitates, owing to the increased solubility.

PRECIPITATE GROWTH MODEL

A precipitate growth model is being developed to predict the formation and evolution of precipitate size distributions in the steel, accounting for kinetic effects. As a first step, accurate PSG methods are developed for both collision and diffusion processes, to simulate precipitate growth in both liquid and solid phases [26]. This PSG method enables a simple calculation of particle growth using only a small number of size groups without losing mass balance. The accuracy of this method is verified by comparison with an exact solution of the primary population balance equation, based on every particle size. It is then applied to simulate distributions in a real steel sample.

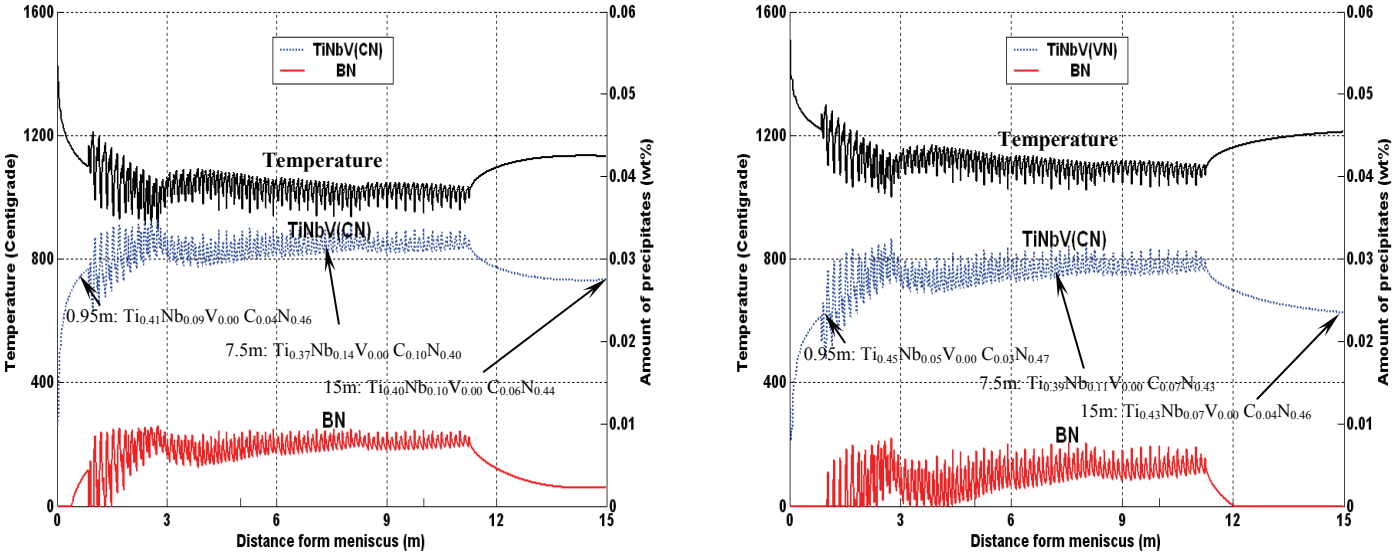

Figure 6. Equilibrium precipitation in 1006 steel continuous cast at 3.7m/min (left) and 5.7m/min (right)

The concept of the PSG method is shown schematically in **Figure 7**. In this method, the particles are divided into groups (group number *j*) with characteristic volume V_j. The threshold volume which separates two neighboring groups is assumed in this work to be the geometric average of the characteristic volumes of these two groups:

$$V_{j,j+1} = \sqrt{V_j V_{j+1}} \tag{3}$$

Where V_j, V_{j+1}: Characteristic (central particle size) volume of group *j* and group *j+1* particle (m^3)

$V_{j,j+1}$: Threshold volume to separate group *j* and group *j+1* particle (m^3)

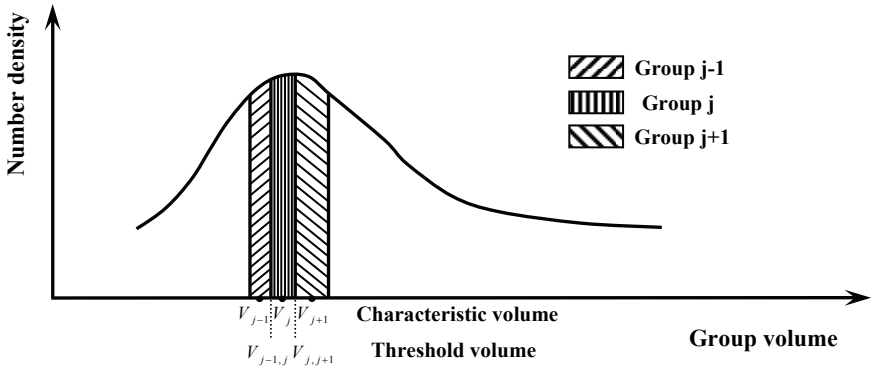

Figure 7: Schematic of particle size distribution in PSG method

If two particles combine to generate a new particle that has a volume between $V_{j-1,j}$ and $V_{j,j+1}$, then the new particle adds to group *j*. If the size of the new particle is different from V_j, the gain in the number density of group *j* is adjusted to match the volume increase. The volume ratio between two neighboring particle size groups, R_V, is defined as

$$R_V = V_{j+1} / V_j \tag{4}$$

The number density of size group *j* particles, N_j, is the number of particles with volume between $V_{j-1,j}$ and $V_{j,j+1}$, per unit volume of steel. By carefully considering the generation and loss terms for each size group, a new PSG method has been developed for both collision and diffusion processes. This work is the first time a PSG method has been applied to diffusion, and it considers both diffusion inside each group and diffusion between groups. Further details are given elsewhere [26].

Collision Model

The general population balance for particle collision was initially introduced by Smoluchowski [10] and a more accurate expression with appropriate corrections is suggested as

$$\frac{dn_i}{dt} = \frac{1}{2}\sum_{k=1}^{i-1}(1+\delta_{k,i-k})\Phi_{k,i-k}n_k n_{i-k} - n_i\sum_{k=1}^{n_M}(1+\delta_{i,k})\Phi_{i,k}n_k \quad (i \geq 2) \tag{5}$$

Where n_i, n_{i-k}, n_k : Number density of size *i* ,*i-k* and *k* particles (/m^3)

$\Phi_{i,j}$: Collision kernel between size *i* and size *j* particles (m^3/s)

$\delta_{i,j}$: Kronecker's delta function, $\delta_{i,j}$=1 for i=j and $\delta_{i,j}$=0 for i≠j

The first term on the right-hand side of equation (5) accounts for the generation of size *i* particles due to collisions of two smaller particles, and the second term accounts for the loss of size *i* particle due to collisions with particles of any size. The generation term is halved because collision pairs are doubly counted.

Validation with Test Problem: Saffman [27] suggested a turbulent collision frequency per unit volume of liquid:

$$\Phi_{ij} = 1.3(\varepsilon/\nu)^{1/2}(r_i + r_j)^3 \tag{6}$$

Where: Φ_{ij} : Collision frequency between size *i* and size *j* particles in unit volume of liquid medium (m^3/s)

ε : Turbulent energy dissipation rate (m^2/s^3)

ν : Kinematic viscosity (m^2/s)

r_i, r_j : Radius of size *i* and size *j* particles (m)

Dimensionless number density of size *i* particles, n_i^*, and dimensionless time, t^*, are defined as:

$$n_i^* = n_i/n_0,\ t^* = 1.3(\varepsilon/\nu)^{1/2}r_1^3 n_0 t \tag{7}$$

Where n_0 : Initial number density of elementary monomers

r_1 : Radius of elementary monomers

t^* : Dimensionless time of turbulence collision

The initial condition is given by n_i^*=1 for i=1 and n_i^*=0 for i>1. The maximum size of agglomerated particle is chosen as n_M=12000, such that 0.1% accuracy in the total volume of particles is guaranteed up to t^*=1. The boundary condition is always that the number density for largest agglomerated particle is zero. Runge-Kutta-Gill method is applied for integration and the time step is Δt^*=0.0025, which is selected by comparing the results from smaller step sizes and finding negligible differences.

Diffusion Model

Particle growth and Ostwald ripening due to diffusion in the solid state are other important processes that determine the precipitate particle size distribution. The diffusion model in this work is similar to the collision model, except that particles can dissociate (shrinking one molecule per time step at most), and interactions are ignored between pairs of particle size groups where both particles are larger than 1 molecule.

The population balance equation for particle size evolution by diffusion is given by Kampmann [28]:

$$\frac{dn_i}{dt} = -\beta_i n_1 n_i + \beta_{i-1}n_1 n_{i-1} - \alpha_i A_i n_i + \alpha_{i+1}A_{i+1}n_{i+1} \quad (i \geq 2) \tag{8}$$

Where n_1, n_{i-1}, n_i, n_{i+1} : Number density of size *1* ,*i-1, i* and *i+1* particles (/m^3)

β_i : Diffusion rate constant of size *i* particles (m^3/s)

α_i : Dissociation rate per unit area of size *i* particles (m^{-2}s^{-1})

A_i : Reaction area of size *i* particles (m^2)

The first and second terms on the right-hand side of equation (8) account for the loss and generation of size *i* particle due to diffusion, while the third and fourth terms for the loss and generation of size *i* particle due to dissociation. The following relations are satisfied for diffusion and dissociation rate [28]

$$\beta_i = 4\pi D_1 r_i,\ \alpha_i = \frac{\beta_i n_1}{A_i} = \frac{\beta_i n_{1,eq}}{A_i}\exp\left(\frac{2\sigma V_m}{RT}\frac{1}{r_i}\right) \tag{9}$$

Where D_1 : Diffusion coefficient of elementary monomers in steel (m^2/s)

r_i : Radius of size *i* particles (m)

$n_{1,eq}$: Number density of the dissolved elementary monomers at equilibrium (/m^3)

σ : Interfacial tension between the precipitate and steel (J/m^2)

V_m : Molar volume of the precipitate (m^3/mol)

R : Ideal gas constant (8.314J·K^{-1}·mol^{-1})

T : Absolute temperature (K)

Note that the exponential decrease in alpha corresponds to the decrease in volume free energy of the new particle relative to the increase in surface energy.

Validation with Test Problem: Choose the dimensionless forms as $n_i^* = n_i / n_{1,eq}$, $t^* = 4\pi D_1 r_1 n_{1,eq} t$ (10)

Where n_i^* : Dimensionless number density of group ***i*** particles

t^* : Dimensionless time of diffusion

Choose parameters $n_{1.eq}=6*10^{23}m^{-3}$, $B=2\sigma V_m/(RTr_1)=3.488$. The initial condition is $n_i^*=0$ for $i\geq 1$ and the boundary condition is also that the number density for largest agglomerated particle is zero all the time. The elementary monomers are produced by an isothermal first order reaction

$$n_s^*(t^*) = n_s(t^*)/n_{1,eq} = \sum_{i=1}^{n_M} i \cdot n_i^* = 9[1-\exp(-0.1t^*)] \quad (11)$$

Where $n_s^*(t^*)$: total dimensionless number density of elementary monomers including those in particles

The maximum size of agglomerated particle is $n_M=1600$, such that the total particle volume is exactly guaranteed up to $t^*=100$. Runge-Kutta-Gill method was also used for integration and the time step is selected as $\Delta t^*=0.005$ for accuracy requirement.

Comparing the PSG method results (points) with the exact solution (lines) for different values of R_V in **Figures 8** and **9**, shows a good match. Comparing left and right frames shows that the accuracy of the PSG method increases with decreasing R_V since more groups are used in the simulation.

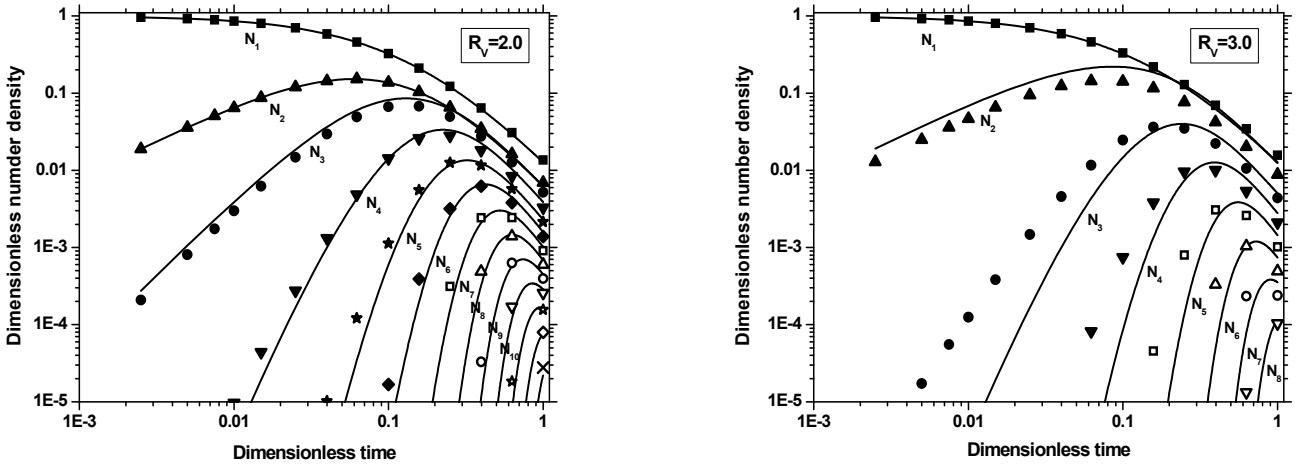

Figure 8: Collision results of each size group by PSG method compared with exact solution for different R_V

Both figures in **Figure 9** show how the size distributions evolve due to the changing concentration gradients near particles of different sizes. At early times, all particle size groups grow, owing to the driving force of increasing supersaturation. At later times, these results show Ostwald ripening. Consider size group N_{10} in $R_V=2$, which contains all of the particle sizes ranging from 363 to 724 molecules, with a central particle size of 512 molecules. The large particles in this particle size group have low concentrations, so tend to grow at the expense of smaller particles, which have high local concentrations, and eventually shrink. For example, size N_1 (1 particle size: 1 molecule) reaches its peak and starts to decrease in number after $t^*=20$.

Sample Results

Figure 10 compares AlN precipitate size distributions predicted for the thin slab product [29]. The simulation starts from the temperature for total dissolution of AlN (1071.8°C, calculated by equilibrium precipitation model) to 900°C assuming the typical cooling rate of 20°C/s given in [30]. The physical parameters are chosen as $V_m=1.33*10^{-5}m^3/mol$, $\sigma=0.75J/m^2$ and diffusion is rate controlled by slow-diffusion element $D_{Al}=3*10^{-3}\exp(-234500/RT)$ from [30]. Constant volume ratio $R_V=2$, 35 size groups and time step $\Delta t=4*10^{-8}s$ are chosen for computation efficiency and stability.

The measured AlN size has a bimodal distribution. The lower-size peak is believed to form due to diffusion, which corresponds with our simulation results, and the larger size peak is believed to happen due to precipitate formation in the segregated liquid between dendrites during solidification or the high diffusion on the grain boundaries due to lots of vacancies and dislocations there.

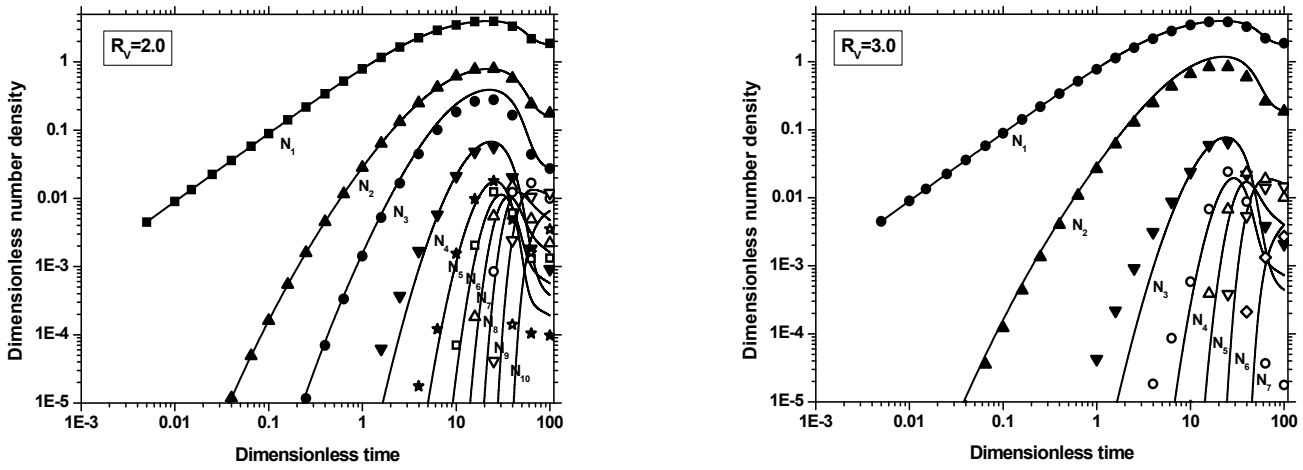

Figure 9: Diffusion results of each size group by PSG method compared with exact solution for different R_V

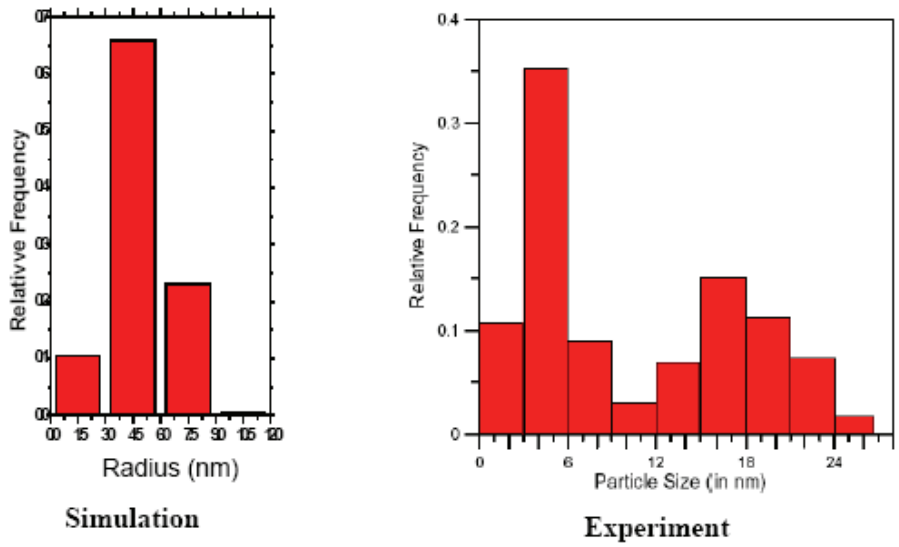

Figure 10: Comparison of AlN size distribution between PSG method and measurement [29]

GRAIN GROWTH MODEL RESULTS

The grain growth model combines a differential equation for grain growth with the pinning effect of precipitates. Thus, its accuracy depends greatly on the equilibrium precipitation and growth models, presented in the previous sections.

Anderson and Grong [18] suggested that grain growth in the presence of precipitates follows:

$$\frac{d\bar{D}}{dt} = M_o^* \exp\left(-\frac{Q_{app}}{RT}\right)\left[\frac{1}{\bar{D}} - \frac{1}{k}\frac{f}{r}\right]^{(1/n-1)} \tag{12}$$

Where $\bar{D}$: Average austenite grain size (m)

M_0^* : Kinetic constant that represents grain boundary mobility

Q_{app} : Apparent activation energy for grain growth (J/mol)

k : Zener coefficient related to the pinning efficiency of the precipitates

f : Volume fraction of the precipitates

r : Radius of the precipitates (m)

n : Exponent to measure resistance to grain boundary motion in the presence of impurities and alloying elements

The driving force for grain growth is reciprocal grain diameter, and it is counteracted by the pinning force which precipitates exert on the boundary. The maximum grain diameter under normal grain growth condition kr/f, called the Zener limit and defined by volume fraction and size distribution of precipitates.

To predict the largest, most detrimental grain size, the pinning force of precipitates is neglected. In this case, the parameters are chosen as $M_0^*=4*10^{-3}m^2/s$, n=0.5 and $Q_{app}=167686+40526*wt\%C_p$ with $wt\%C_p=wt\%C-0.14wt\%Si+0.04wt\%Mn$ from experimental fitting over a wide range of steel compositions [21]. The initial austenite grain size at start temperature of totally austenite structure (1410.9°C) is assumed to be the primary dendrite arm spacing (PDAS) of approximately $\lambda_1 \approx 185\mu m$, based on cooling rate $C_R=104^oC/s$ for both casting speeds using the empirical formula in reference [31]. Equation (12) is then integrated along distance from the meniscus. The Runge-Kutta method is used with time step $\Delta t=0.125s$ for accuracy. **Figure 11** shows results for the slab surface grain size of 1006 steel cast at 3.7 and 5.7m/min. Without consideration of precipitates, the surface grains approaches 50% of their final size by mold exit and are large enough to cause cracks. The temperature under oscillation marks is taken as that of 0.5mm (typical oscillation depth) below surface. This produces grain sizes at oscillation marks of ~ 10% larger than on the surface at the end of casting for both casting speeds. At 10mm below the surface, the grains are almost as twice larger as surface grains.

At higher casting speed (5.7m/min), although time in the caster is shorter, the grain size near the surface is even larger than at lower casting speed (3.7m/min). This is because the temperature is much higher. Thus the secondary spray water cooling rates must be carefully chosen to control the grain size for a given casting speed.

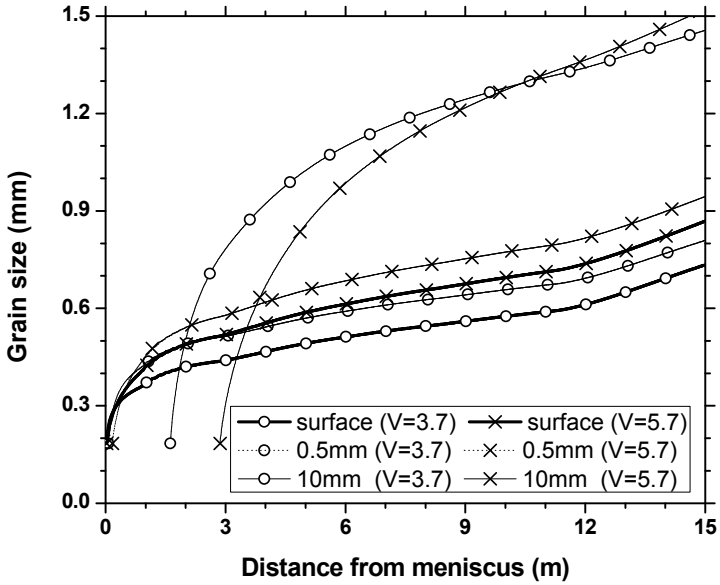

Figure 11: Grain size simulation of 1006 steel at different depths and casting speeds

But from the equilibrium precipitation calculation, precipitates are seen to form as early as in the mold. As an rough estimation, the corresponding volume fraction of stable TiN is approximately $2.6*10^{-4}$ at mold exit by choosing $\rho_{steel}=7500kg/m^3$ and $\rho_{TiN}=5420kg/m^3$. Assuming a typical average TiN particle size of 10~100nm and k=4/3, as proposed originally by Zener and Smith in 1948, the maximum grain size is calculated in the range of 50~500μm. Clearly, precipitates usually play an important role in refining the austenite grain size and will be the focus of future coupled modeling.

CONCLUSIONS

1). An equilibrium precipitation model is established, which includes the solubility limit of each precipitate with influence of activities from interaction of elements in steels, mutually soluble or exclusive properties between precipitates and complete mass balance of all elements before and after precipitation. The model is applied for 1006 steel under continuous casting process. Among the major precipitates during austenite phase, TiN is the most stable precipitate due to its lowest solubility limit. After nitrogen is combined with more stable nitrides and still plenty of free carbon available, NbC becomes important because of its low ratio of solubility products of the carbide and nitride of Nb. If there is enough Ti and S, then Ti sulphide and carbosulphide are also commonly observed.
2). The PSG method is validated for particle agglomeration due to collision and diffusion. Within a wide range of volume ratios, R_V, mass balance is satisfied and a good match is found between exact solution and PSG method. Because the accuracy of the PSG method increases with decreasing R_V, an R_V of 2.0 seems optimal.
3). Without sacrificing accuracy, the PSG method needs only a small number of size groups to simulate the size distribution of AlN precipitates in thin slab casting. The computed distribution matches with the smaller peak of the measured bimodal distribution, agreeing with the two-fold mechanism that precipitate sizes form during solidification, and later due to solid-state diffusion.
4). A grain growth model is presented that starts when austenite first forms, assuming primary dendrite arm spacing as initial grain size. In continuous casting, the model predicts grains approaching 50% of their final size by mold exit. The grains under oscillation marks are at least 10% larger than those on the slab surface due to local high temperature. Without precipitates, the grains are large enough to cause ductility problems.
5). The higher temperature and the corresponding larger grain growth rate and lack of fine precipitates are likely the controlling factors to cause coarse grains and susceptibility to surface cracks especially beneath oscillation marks.

ACKNOWLEDGEMENTS

The authors wish to thank members of the Continuous Casting Consortium at the University of Illinois at Urbana-Champaign (UIUC) and the National Science Foundation (Grant DMI 05-00453) for their continuous financial support of the research.

REFERENCES

1. E. S. Szekeres, *6th Internat. Conf. on Clean Steel*, Balatonfüred, Hungary, June 2002.
2. W. J. Liu, J. J. Jonas and E. B. Hawbolt, Thermodynamic Prediction of Carbonitride and Sulphide Precipitation in Multicomponent Austenite, 29th Annual Conference of Metallurgists, Hamilton, 1990, 457-466.
3. J. Y. Park, J. K. Park and W. Y. Choo, Effect of Ti Addition on the Potency of MnS for Ferrite Nucleation in C-Mn-V Steels, *ISIJ International*, 2000, vol.40, 1253-1259.
4. N. Yoshinaga, K. Ushioda, S. Akamatsu and O. Akisue, Precipitation Behavior of Sulfides in Ti-added Ultra Low-carbon Steels in Austenite, ISIJ International, 1994, vol.34, 24-32.
5. E. E. Kashif, K. Asakura, T. Koseki and K. Shibata, Effect of Boron, Niobium on Grain Growth in Ultra High Purity 18% Cr Ferritic Stainless Steel, *ISIJ International*, 2004, vol.44, 1568-1575.
6. J. Y. Choi, B. S. Seong, S. C. Baik and H. C. Lee, Precipitation and Recrystallization Behavior in Extra Low Carbon Steels, ISIJ International, 2002, vol.42, 889-893.
7. B. J. Lee, Thermodynamic Assessment of the Fe-Nb-Ti-C-N system, *Metallurgical and Materials Transactions A*, 2001, vol.32, 2423-2439.
8. S. C. Park, I. H. Jung, K. S. OH and H. G. LEE, Effect of Al on the Evolution of Non-metallic Inclusions in the Mn-Si-Ti-Mg Deoxidized Steel During Solidification: Experiments and Thermodynamic Calculations, *ISIJ international*, 2004, vol.44, 1016-1023.
9. Y. Li, J. A. Wilson, D. N. Crowther, P. S. Mitchell, A. J. Craven and T. N. Baker, The Effect of Vanadium, Niobium, Titanium and Zirconium on the Microstructure and Mechanical Properties of Thin Slab Cast Steels, *ISIJ International*, 2004, vol.44, 1093-1102.
10. M. Smoluchowski, Versuch Einer Mathematischen Theorie der Koagulationskinetic Kolloider Losungen, *Z. Phys. Chem.*, 92, 1917, 127~155.
11. K. Nakanishi and J. Szekely, Deoxidation kinetics in a turbulent flow field, *Transactions ISIJ*, 15, 1975, 522-530.
12. U. Lindborg and K. Torssell, A collision model for the growth and separation of deoxidation products, *Transactions of Metallurgical Society of AIME*, 242, 1968, 94-102.
13. W. Ostwald, *Lehrbruck der allgemeinen Chemie*, Vol. 2, 1896, Leipzig, Germany.
14. I. M. Lifshitz and V. V. Slyozov, The kinetics of precipitation from supersaturated solid solutions, *Journal of Physics and Chemistry of Solids*, 19, 1961, 35-50.
15. C. Wagner, Theorie der alterung von niederschlägen durch umloesen, *Zeitschrift Zeitschr. Elektrochemie*, 65, 1961, 581-591.
16. T. Nakaoka, S. Taniguchi, K. Matsumoto and S. T. Johansen, Particle-Size-Grouping method of inclusion agglomeration and its application to water model experiments, *ISIJ international*, 41, 2001, 1103-1111.
17. N. Zhang and Z. C. Zheng, A collision model for a large number of particles with significantly different sizes, *Journal of Physics D: Applied Physics*, 40, 2007, 2603-2612.

18. I. Andersen and Ø Grong, Analytical Modelling of Grain Growth in Metals and Alloys in the Presence of Growing and Dissolving Precipitates–I. Normal Grain Growth, *Acta Metallurgica Materialia*, 1995, vol. 43, 2673-2688.
19. I. Andersen, Ø Grong and N. Ryum, Analytical Modelling of Grain Growth in Metals and Alloys in the Presence of Growing and Dissolving Precipitates–II. Abnormal Grain Growth, *Acta Metallurgica Materialia*, 1995, vol. 43, 2689-2700.
20. J. Reiter, C. Bernhard and H. Presslinger, Austenite Grain Size in the Continuous Casting Process: Metallographic Methods and Evaluation, *Materials Characterization*, 2008, vol. 59, 737-746.
21. J. Reiter, C. Bernhard and H. Presslinger, Determination and Prediction of Austenite Grain Size in Relation to Product Quality of the continuous Casting Process, *Materials Science & Technology (MS&T), Conference and Exhibition, Cincinnati, USA*, 2006, 805-816.
22. Y. Meng and B. G. Thomas, Heat Transfer and Solidification Model of Continuous Slab Casting: CON1D, *Metallurgical and Materials Transactions B*, 2003, vol. 34B, 685-705.
23. Y. M. Won and B. G. Thomas, Simple Model of Microsegregation during Solidification of Steels, *Metallurgical and Materials Transactions A*, 2001, vol. 32A, 1755-1767.
24. K. Zheng, B. Petrus, B. G. Thomas and J. Bentsman, Design and Implementation of a Real-time Spray Cooling Control System for Continuous Casting of Thin Steel Slabs, AISTech 2007, Steelmaking Conference Proc., (May, Indianapolis, IN), AIST, Warrendale, PA, vol. 1.
25. K. Xu, Modeling of Precipitate Formation in Continuous Steel Casting, *Continuous Casting Consortium Annual Report,* UIUC, 2007.
26. K. Xu, Modeling Heat Transfer, Precipitate Formation and Grain Growth during Secondary Spray Cooling, *Continuous Casting Consortium Annual Report,* UIUC, 2008.
27. P. G. Saffman and J. S. Turner, On the Collision of Drops in Turbulent Clouds, *Journal of Fluid Mechanics*, 1, 1956, 16-30.
28. L. Kampmann, M. Kahlweit, On the Theory of Precipitation II, *Berichte der Bunsen-Gesellschaft Physikalische Chemie*, 74(5), 1970, 456-462.
29. J. A. Garrison, Aluminum nitride precipitation behavior in thin slab material, AIST 2005 proceeding, volume II, June 2002.
30. Y. Kand, H. Yu, J. Fu, K. Wang, Z. Wang, Morphplogy and Precipitation Kinetics of AlN in Hot Strip of Low Carbon Steel Produced by Compact Strip Production, Materials Science and Engineering A, 2003, vol. 351, 265-271.
31. M. E. Bealy and B. G. Thomas, Prediction of Dendrite Arm Spacing for Low Alloy Steel Casting Processes, *Metallurgical and Materials Transactions B*, 1996, vol. 27B, 689-693.